Title

Affinity of small-molecule solutes to hydrophobic, hydrophilic, and chemically patterned interfaces in aqueous solution

Journal

Proceedings of the National Academy of Sciences of the United States of America, 118(1)

ISSN

0027-8424

Authors

Monroe, Jacob I
Jiao, Sally
Davis, R Justin
et al.

Publication Date

2021-01-05

DOI

10.1073/pnas.2020205118

Peer reviewed

Affinity of small-molecule solutes to hydrophobic, hydrophilic, and chemically patterned interfaces in aqueous solution

Jacob I. Monroe[a], Sally Jiao[a], R. Justin Davis[b], Dennis Robinson Brown[a], Lynn E. Katz[b], and M. Scott Shell[a,1]

[a]Department of Chemical Engineering, University of California, Santa Barbara, CA 93106; and [b]Department of Civil, Architectural and Environmental Engineering, University of Texas at Austin, Austin, TX 78712

Edited by Peter J. Rossky, Rice University, Houston, TX, and approved November 17, 2020 (received for review September 30, 2020)

Performance of membranes for water purification is highly influenced by the interactions of solvated species with membrane surfaces, including surface adsorption of solutes upon fouling. Current efforts toward fouling-resistant membranes often pursue surface hydrophilization, frequently motivated by macroscopic measures of hydrophilicity, because hydrophobicity is thought to increase solute–surface affinity. While this heuristic has driven diverse membrane functionalization strategies, here we build on advances in the theory of hydrophobicity to critically examine the relevance of macroscopic characterizations of solute–surface affinity. Specifically, we use molecular simulations to quantify the affinities to model hydroxyl- and methyl-functionalized surfaces of small, chemically diverse, charge-neutral solutes represented in produced water. We show that surface affinities correlate poorly with two conventional measures of solute hydrophobicity, gas-phase water solubility and oil–water partitioning. Moreover, we find that all solutes show attraction to the hydrophobic surface and most to the hydrophilic one, in contrast to macroscopically based hydrophobicity heuristics. We explain these results by decomposing affinities into direct solute interaction energies (which dominate on hydroxyl surfaces) and water restructuring penalties (which dominate on methyl surfaces). Finally, we use an inverse design algorithm to show how heterogeneous surfaces, with multiple functional groups, can be patterned to manipulate solute affinity and selectivity. These findings, importantly based on a range of solute and surface chemistries, illustrate that conventional macroscopic hydrophobicity metrics can fail to predict solute–surface affinity, and that molecular-scale surface chemical patterning significantly influences affinity—suggesting design opportunities for water purification membranes and other engineered interfaces involving aqueous solute–surface interactions.

inverse design | molecular simulation | membrane fouling | solvation free energy | surface adsorption

Increasing global population, rising urbanization, and climate change pose tremendous constraints on the food, energy, and water sectors, with demands for these inextricably linked resources expected to grow by 60%, 80%, and 55%, respectively, by 2050 (1). Technologies attacking the linkages among these sectors must be developed, and within the water sector, these include low-energy treatment processes that transform low-quality waters into (re)usable water sources for agriculture, energy, and industry. Membrane processes are promising for minimizing energy expenditures (2, 3), but transformative improvements require a deep understanding of solute–surface molecular interactions that control water permeation, separation selectivity, and membrane fouling (4, 5). For example, pioneering work (6) suggests that antifouling surfaces be hydrophilic, charge neutral, and avoid hydrogen bond donating groups, and many antifouling strategies have emerged on this basis (7–9). The emphasis on hydrophilizing surfaces relies on the hypothesis that such interfaces tightly bind water that resists displacement by solutes (10).

However, a molecular understanding that links membrane surface chemistry to solute affinity and hence membrane functional properties remains incomplete, due in part to the complex interplay among specific interactions (e.g., hydrogen bonds, electrostatics, dispersion) and molecular morphology (e.g., surface and polymer configurations) that are difficult to disentangle (11–14). Chemically heterogeneous surfaces are even less understood but can affect fouling in complex ways. For example, in amphiphilic surfaces, hydrophilic groups are thought to aid antifouling while hydrophobic ones provide foulant release (15), and several studies have examined solute adsorption in response to variations in the composition of functional groups at a surface (16–19). These observations suggest that functional surfaces may require heterogeneous chemical composition, and recent theory supports the promise and complexity of such surfaces; for example, the spatial arrangement or patterning of heterogeneous surface chemical groups strongly influences the thermodynamic (20–24) and dynamic (25) properties of surface hydration water. Broadly, rational engineering of complex surface chemical functionalization to control solute–surface affinity requires fundamental molecular insight and guiding principles.

Theoretical work has informed solute–surface affinity for a variety of experimental systems of interest. For example,

Significance

Increasing global population, urbanization, and climate change pose tremendous constraints on water availability. While membrane processes offer attractive, energy-efficient options, transformative advances in membrane technology are needed to enable reuse of poor-quality waters from diverse sources. This work brings fundamental understanding of solute–surface interactions to membrane phenomena, including selectivity and fouling. Molecular simulations reveal limitations of traditional predictive measures of solute–surface partitioning, suggesting alternative thermodynamic signatures for solute binding that highlight the contextual nature of hydrophobicity. An inverse design algorithm provides a tool to pattern membrane nanoscale chemistry to optimize solute affinity and selectivity. This work demonstrates how simulations can inform practical materials design for sustainable water treatment and, more broadly, many technologies involving water-mediated solute–surface interactions.

Author contributions: J.I.M., L.E.K., and M.S.S. designed research; J.I.M., S.J., R.J.D., D.R.B., and M.S.S. performed research; J.I.M., S.J., R.J.D., D.R.B., L.E.K., and M.S.S. analyzed data; and J.I.M., S.J., R.J.D., D.R.B., L.E.K., and M.S.S. wrote the paper.

The authors declare no competing interest.

This article is a PNAS Direct Submission.

[1]To whom correspondence may be addressed. Email: shell@engineering.ucsb.edu.

This article contains supporting information online at https://www.pnas.org/lookup/suppl/doi:10.1073/pnas.2020205118/-/DCSupplemental.

Published December 28, 2020.

simulation fouling studies have examined the adsorption of large and chemically heterogeneous protein and peptide solutes on self-assembled monolayer (SAM) (17, 26–32), mineral (33, 34), and graphene (35, 36) surfaces, primarily focused on chemically homogeneous surfaces. Other efforts have specifically addressed the role of solute chemistry; for example, studies of adsorption on graphene identified thermodynamic trends driving solute binding (37, 38), and developed predictive models based on solute molecular descriptors (39). Many such studies have focused in particular on aromatic compounds, which exhibit strong affinity for graphenic interfaces (40).

At the same time, the past decades have seen significant advances in the molecular theory of hydrophobicity, originating with models and simulations of idealized (e.g., hard sphere) solutes (41–43) and moving toward chemically complex interfaces, particularly those of biomolecules (44–47). Adsorption of simple solutes at idealized and biological surfaces has been connected to water density fluctuations (21, 47), with recent theories classifying surface hydrophobicity by this quantity within probe volumes at interfaces (20, 42, 43). Studies of ligand binding to relatively rigid, chemically complex protein binding pockets (48, 49) and of protein dimerization (44, 50–52) have further emphasized the role of water structure and density fluctuations in driving association. Related efforts have examined association of larger surface moieties (44, 53, 54), including chemically heterogeneous protein surfaces (52, 55), showing the potential relevance of larger water density fluctuations such as dewetting. These efforts provide valuable, although largely unleveraged, information for the design of membrane interfaces, emphasizing the influence of water's structural (e.g., tetrahedral) behavior and density fluctuations (including molecular dewetting) on solute–solute and solute–surface interactions, and suggesting the failure of macroscopic models built on, for example, solute surface area and volume (56–58).

These insights demand a broader investigation of the complex role of chemistry in water-mediated solute–surface interactions to establish molecular design rules for synthetic surfaces like those of membranes that in particular involve a highly diverse range of relevant solute and surface functionalization chemistries, including chemically heterogeneous surfaces. The present work therefore seeks to provide a systematic examination of the combined roles of solute and surface chemistries on surface affinity of molecular solutes, spanning a wide range of realistic chemical moieties (hydrophobic to hydrophilic) and exploring both homogeneous and heterogeneous, patterned surfaces. As model interfaces, we simulate well-studied (25, 28, 36, 43, 59) models of alkanethiol SAMs with hydroxyl and methyl headgroups, representing idealized hydrophilic and hydrophobic surfaces, as well as SAMs with positively (quaternary ammonium) and negatively (sulfonate) charged headgroups, common functionalities in membrane surface engineering. In all cases, the surfaces are planar, which allows us to isolate the effects of chemistry independent of surface geometry, which separately is known to impact hydrophobicity and solute binding (60–63).

We consider a chemically diverse set of small solutes (Table 1) relevant to produced water separations (2, 3). Here, we limit our investigation to uncharged solutes, focusing on physical trends that avoid ion-specific behaviors that are actively investigated (64). Building on advances in hydrophobicity theory suggesting the relevance of water density fluctuations near hydrophobic surfaces (20, 21, 42, 43, 47), we establish that such fluctuations signal solute surface binding even across a wide range of solute chemistries and surface types. Moreover, we propose that surface affinity across this chemistry spectrum is naturally described by a decomposition of thermodynamic driving forces that decouples direct energetic (interaction) contributions from water restructuring penalties. Finally, we use an inverse design algorithm to discover chemically patterned surfaces that have extremal affinity or selectivity and show that such surfaces offer an attractive strategy for tuning these properties.

Methods

Model Systems. Simulation SAM models were described previously (25, 28, 32, 65). Detailed descriptions of surface parameters are provided in *SI Appendix*. We apply periodic boundary conditions to the 2.9820 × 3.4432 × 6.0000-nm SAM systems, which gives ∼3.5 nm of water between SAM layers. For solutes in bulk water, simulation boxes are 3.5 × 3.5 × 3.5 nm. Water is modeled as TIP4P/Ew (66), and most solutes use AMBER GAFF2 parameters (67) with AM1-BCC charges (68) generated through ANTECHAMBER. For capped glycine, we use the AMBER ff14SB force field (69). Boric acid parameters are from several sources (67, 70, 71). To determine solvation free energies in octanol, we construct 3.5 × 3.5 × 3.5-nm boxes with single solutes and octanol solvent modeled by the united-atom TRAPPE force field (72), with all bonds constrained. Further model details are found in *SI Appendix*.

Molecular Dynamics Simulations and Free Energy Calculations. All molecular dynamics (MD) simulations utilize GPU-accelerated OpenMM (73), with waters constrained by SETTLE (74), nonwater bonds involving hydrogens constrained by SHAKE (75), and equations of motion propagated via a 2-fs time step with Langevin dynamics. We apply an isotropic Monte Carlo barostat in bulk systems, and an anisotropic barostat to the z dimension (normal to the interface) in SAM systems. Particle mesh Ewald handles long-range electrostatics, and we apply a hard 1.2-nm real-space cutoff to both coulombic and Lennard–Jones (LJ) interactions with no dispersion corrections.

We compute potentials of mean force (PMFs) using umbrella sampling (76) with solute heavy-atom centroids restrained with a harmonic potential at increasing distances from the interface. Umbrella starting configurations are drawn from a solute pulling simulation, and we then equilibrate each umbrella in the NVT ensemble for 500 ps and for 1 ns in the NPT ensemble, before 10-ns production runs.

To compute solvation free energies, we employ expanded ensemble techniques (77, 78) with Monte Carlo moves between solute–system interaction states every 250 time steps (0.5 ps). States span the solute fully interacting with the system (state 1) to fully decoupled (state 2); the free energy from state 1 to state 2 is that to solvate an ideal gas solute in the same volume occupied by the uncoupled system. Fine details of the expanded ensemble procedure are in *SI Appendix*.

We separate solvation free energies into contributions from LJ repulsions, LJ attractions, and electrostatic interactions using reweighting via MBAR (79). Specifically, this provides the free energy to move a solute from an ideal gas to solution interacting via only a Weeks–Chandler–Andersen potential (80), from this point to interacting with LJ interactions, and finally from this point to full interactions including electrostatics. We calculate relative entropies associated with each of these processes by combining free energies with weighted averaging of potential energies.

To quantify the role of density fluctuations, we consider the probability distribution $P(N)$ for the number of water oxygens N in methane-sized probes of radius 0.33 nm. Notably, the zero-water, or cavity, probability is related to the excess chemical potential of solvating a methane-sized hard-sphere solute, $\mu_{ex}^{HS} = -k_BT \ln P(N = 0)$. For a Gaussian fluctuation spectrum, this quantity then relates to the mean water density and density variance per the following relationship (81, 82): $-\ln P(N = 0) \approx \langle N \rangle^2 / 2\sigma_N^2$.

Genetic Algorithm Optimization. We develop a genetic algorithm to make affinity optimization possible by adjusting surface patterns, which minimizes the binding free energy (equivalently, surface free energy) by using MD simulations to calculate this quantity for each candidate surface pattern. A similar approach was described previously (25), although here we accelerate it using an on-the-fly machine-learned surrogate model for the solvation free energy, which is critical to the exploration of pattern space due to the expense of free energy calculations. Briefly, the genetic algorithm treats each surface pattern as an "individual" with a specific level of "fitness," such as a solute's binding free energy. The algorithm then evolves a population of surfaces by combining and randomly adjusting ("mutating") surface patterns, to identify surface patterns that minimize or maximize solute surface affinity, or alternately selectivity as defined by the difference in surface affinity of two distinct solutes. *SI Appendix*, Fig. S1 illustrates the procedure, which involves stages iterating between detailed evaluation of binding free energies with expanded ensemble MD and rapid evaluation of the same via the on-the-fly-learned machine-learned model. This model is built with LASSO regression and predicts free energies based on the surface patterns alone, without need for simulation. It is first trained on 128 surface patterns

Table 1. Solute structures and solvation free energies

Solute	Structure	$\Delta G_{solv}^{CH_3}$	ΔG_{solv}^{OH}	ΔG_{solv}^{bulk}	ΔG_{solv}^{Henry}
Ammonia		−8.32 ± 0.06	−7.59 ± 0.03	−7.53 ± 0.07	−7.3 (5.9×10^{-1})
Benzene	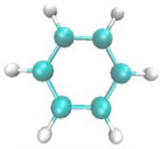	−5.59 ± 0.07	−2.37 ± 0.07	−1.20 ± 0.07	−1.4 (1.7×10^{-3})
Boric acid	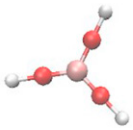	−8.47 ± 0.06	−7.61 ± 0.12	−7.24 ± 0.09	−23.0 (3.8×10^{6})*
Capped glycine	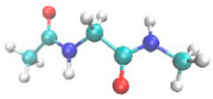	−27.62 ± 0.16	−25.17 ± 0.14	−23.87 ± 0.09	N/A
Isopropanol	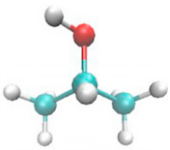	−14.37 ± 0.05	−11.72 ± 0.06	−10.73 ± 0.07	−8.1 (1.3×10^{0})
Methane		1.09 ± 0.02	3.41 ± 0.05	3.95 ± 0.06	3.36 (1.4×10^{-5})
Methanol	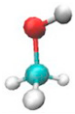	−12.50 ± 0.01	−10.89 ± 0.13	−10.44 ± 0.09	−8.5 (2.0×10^{0})
Phenol	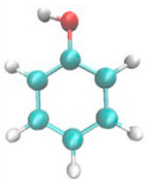	−16.69 ± 0.07	−13.30 ± 0.11	−12.15 ± 0.12	−11.1 (2.8×10^{1})

Solvation free energies as reported correspond to bulk or when the solute is near methylated (CH_3) or hydroxylated (OH) SAM surfaces. Units are reported in k_BT with uncertainties based on five independent runs. In the last column, solvation free energies are computed from Henry's law constants; the latter are shown in parentheses (units of moles per cubic meter·pascal) and obtained from ref. 104. For an accurate force field, the last two columns should be equal. See *SI Appendix* for a full derivation.

*The Henry's law constant for boric acid is approximated from vapor pressure of the pure substance divided by the aqueous solubility, a less precise technique compared to those used for other solutes.

explored in an initial stage of explicit free energy calculations; as the genetic optimization proceeds, it is then periodically retrained with further explicit calculations on newly explored surface motifs. Details of this procedure are in *SI Appendix*.

Results and Discussion

Diverse Solute Chemistries Show Affinity for Both Polar and Nonpolar Surfaces. While hydrophobic solutes are well known to adhere to hydrophobic interfaces, what level of surface polarity or overall hydrophilicity is required to prevent such binding? Conversely, a more polar surface may strongly bind water that creates a barrier to adsorption of nonpolar solutes (43, 83), but the effect on polar solutes is less clear due to potential complementary electrostatic interactions (51). To address such questions, we consider a diverse range of small solutes represented in produced water spanning nonpolar (e.g., benzene) to polar (e.g., ammonia), as shown in Table 1. We first evaluate the interactions of these solutes with SAM surfaces of either methylated (CH_3) or hydroxylated (OH) headgroups—model systems that represent conventionally considered "ideal" hydrophilic and hydrophobic surfaces. To determine surface affinities, we calculate the free energy to transfer a solute from an ideal gas state to a solvated state, ΔG_{solv}, separately in bulk solution and at a given interface. The surface binding free energy is then as follows:

$$\Delta G_{bind} = \Delta G_{solv}^{surf} - \Delta G_{solv}^{bulk}, \quad [1]$$

which bears direct relation to the relative surface solute concentration under dilute conditions, $c^{surf}/c^{bulk} = \exp(-\Delta G_{bind}/k_BT)$,

such that negative ΔG_{bind} values imply surfaces enriched with solutes relative to bulk.

What characterizes the hydrophobicity of a solute in this surface-binding context? We find that conventional solution-phase metrics correlate poorly with surface affinity via Eq. **1**. One classic hydrophobicity measure is the bulk solvation free energy ΔG^{bulk}_{solv}, which gives a solute's excess chemical potential at infinite dilution in bulk solution, and is directly related to its Henry's law constant (84, 85). All of the solutes studied except for methane exhibit negative bulk solvation free energies (Table 1). While intuitively one might expect that solutes more difficult to solvate should have higher affinity to the hydrophobic methyl surface, Fig. 1*A* reveals that ΔG^{bulk}_{solv} is unrelated to ΔG_{bind}. While unexpected for entropically driven affinity of purely repulsive solutes (81, 86), this is in line with differences in solute association observed with the addition of dispersive attractive interactions (41, 53, 87–89), although the solutes considered here span a much wider range of chemistries and molecular shapes than has been investigated.

Oil–water partition coefficients—commonly used to calibrate hydrophobicity in biophysical studies and to predict affinities in reversed-phase chromatography (90) among many other applications—similarly poorly predict binding affinities. Specifically, we compute the logarithm of these partition coefficients, equal to the difference in solvation free energies for a solute in water and octanol phases. As Fig. 1*B* shows, we find better agreement between binding affinities and octanol–water transfer free energies, but only for the methylated interface, and the trend disappears when the most polar solutes are omitted. Thus, for the small solutes studied, the present calculations suggest that surface affinity is not well predicted by these conventional and widely studied measures of solute hydrophobicity.

Fig. 2 shows the binding landscapes as PMFs that give the free energy (or infinite-dilution excess chemical potential) as a function of solute heavy-atom centroid distance to the interface. Interestingly, the PMFs show that all solutes have a free energy minimum and thus some affinity for both the methylated and hydroxylated interfaces, although the affinity is nearly negligible for ammonia and boric acid near the hydroxylated surface. Still, even solutes often considered hydrophilic and that can hydrogen bond with water show a decrease in free energy as they approach the hydrophobic, methylated surface. A similar water-induced attraction has been shown to be possible for the case of

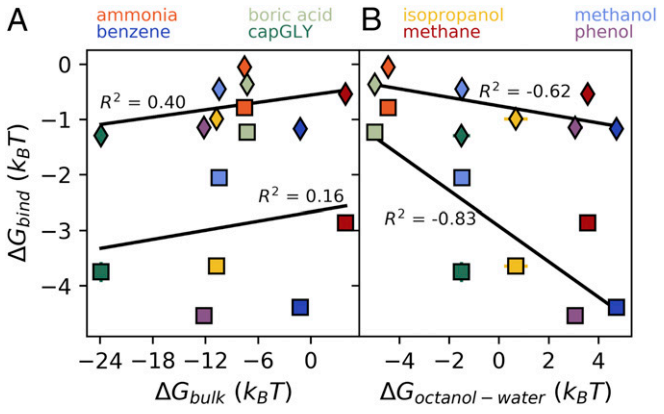

Fig. 1. Binding free energies at interfaces are poorly correlated with bulk solvation free energies (*A*). Correlations improve when comparing binding free energies to octanol–water transfer free energies (*B*), but only for the methylated surface and only if boric acid and ammonia, the most polar solutes, are included. Diamonds represent fully hydroxylated interfaces, while squares are fully methylated.

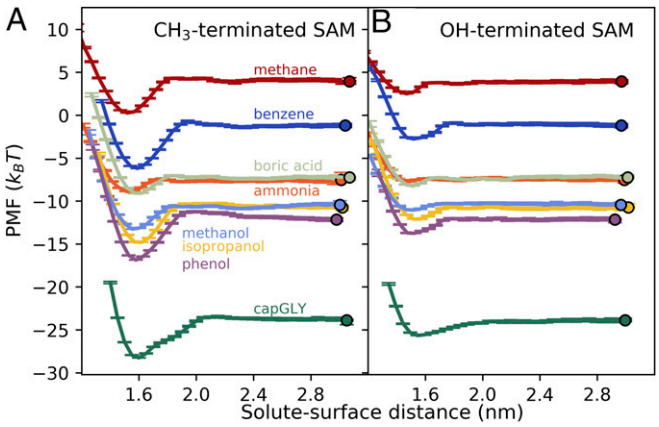

Fig. 2. Potentials of mean force (PMFs) for all solutes studied at (*A*) methylated and (*B*) hydroxylated interfaces. The distance to the interface is calculated from the solute heavy-atom centroid to the fixed sulfur atoms of the SAM chains. PMF values are relative to the bulk solvation free energies of solutes, which are shown as points at the furthest distances from the interface sampled. Error bars are those reported by pymbar (68).

associating extended surfaces, one polar and one nonpolar (91, 92). Furthermore, an attraction of peptides to hydrophilic SAM surfaces has also been observed, both in simulation and experimentally (27, 28, 36).

To understand these results, we decompose solvation free energies into contributions from distinct intermolecular interactions, $\Delta G_{solv} = \Delta G_{rep} + \Delta G_{attr} + \Delta G_Q$, in a three-step process: 1) ΔG_{rep} for turning on purely repulsive solute–system interactions from the fully decoupled state (solute in the ideal gas phase), 2) ΔG_{attr} for then adding attractive LJ interactions, and 3) ΔG_Q for introducing electrostatics to the LJ solute. Decompositions of this form are commonly used to understand solvation and ligand binding, especially in biomolecular contexts (58). *SI Appendix*, Fig. S4 reports these quantities both in bulk and at methylated and hydroxylated interfaces. With Eq. **1**, we obtain a similar breakdown of contributions upon binding (58):

$$\Delta G_{bind} = \left(\Delta G^{surf}_{rep} - \Delta G^{bulk}_{rep}\right) + \left(\Delta G^{surf}_{attr} - \Delta G^{bulk}_{attr}\right) + \left(\Delta G^{surf}_{Q} - \Delta G^{bulk}_{Q}\right) = \Delta\Delta G_{rep} + \Delta\Delta G_{attr} + \Delta\Delta G_{Q}. \quad [2]$$

Fig. 3*A* shows that, at the methylated interface, $\Delta\Delta G_{attr}$ and $\Delta\Delta G_Q$ are positive for all solutes, disfavoring adsorption, but ultimately binding is driven by dominating, negative $\Delta\Delta G_{rep}$ values. Indeed, all of these small solutes are expected to induce unfavorable entropic penalties when solvated in bulk due to excluded volume effects with surrounding water (81). These penalties shrink in the methylated interfacial region, where water density is depressed and relative density fluctuations grow, creating a higher probability of spontaneous water-free cavities in which the solute may reside (45, 93) and a net driving force for binding (49, 94). This is certainly expected based on past studies of idealized hydrophobic solutes (41, 87), but here we demonstrate that this contribution also primarily drives affinity for a variety of polar ones. It might seem intuitively reasonable that methanol, isopropanol, and phenol manifest affinity for the methylated interface, as they can reorient their hydroxyl group away from the surface to maintain hydrogen bonds with water. However, even ammonia and boric acid exhibit surface adsorption driven by $\Delta\Delta G_{rep}$, and both sacrifice hydrogen bonds upon moving to the methylated surface, as indicated by positive $\Delta\Delta G_Q$.

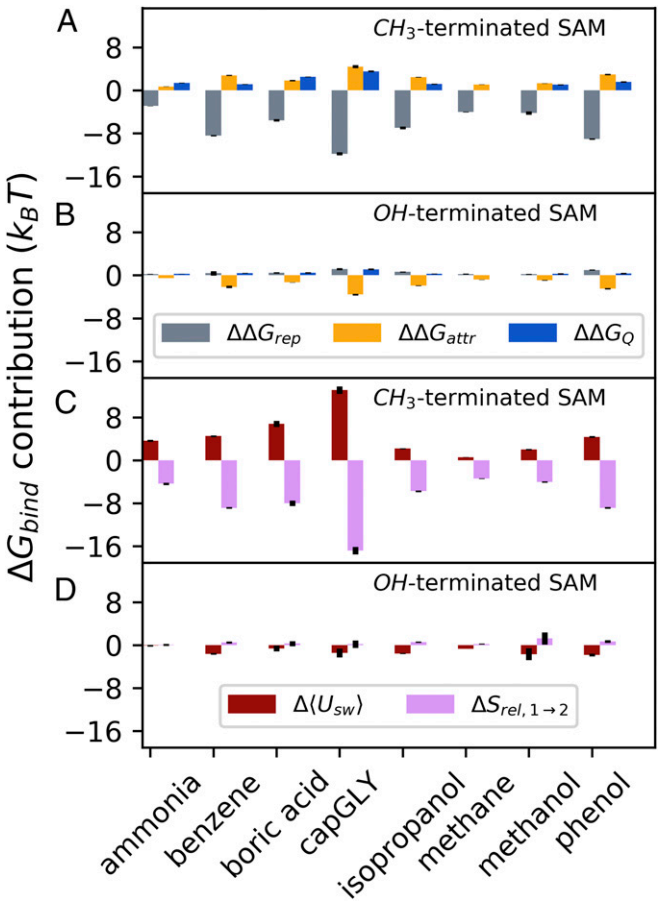

Fig. 3. Contributions to binding free energies as described in the text and defined in Eqs. **2** and **3** for the (*A*) methylated and (*B*) hydroxylated SAM surfaces. Summing the $\Delta\Delta G_{rep}$ and $\Delta\Delta G_{attr}$ yields the change in LJ interactions $\Delta\Delta G_{LJ}$. The repulsive component, which involves creating a cavity in which the solute may be inserted, is the predominant thermodynamic driving force for a solute's preference for the interface over bulk solution. *C* and *D* show free energies of binding broken into differences between direct solute–system energetics ($\Delta\langle U_{sw}\rangle_2$) of solvation and relative entropies of solvation ($\Delta S_{rel,1\to2}$), which for relatively rigid surfaces and solutes are dominated by water restructuring due to a solute.

In direct contrast, Fig. 3*B* indicates that at the hydroxyl interface it is instead $\Delta\Delta G_{attr}$ that drives affinity, while $\Delta\Delta G_{rep}$ values are small and positive. The large negative $\Delta\Delta G_{attr}$ contribution is likely due to the higher LJ energy density of the SAM surface compared to bulk water, as well as the increased density of water in the spatial region where the solutes bind (e.g., the PMF minima) (*SI Appendix*, Fig. S8). Conversely, at the methylated interface, $\Delta\Delta G_{attr}$ is positive because solutes bind in a ∼0.25-nm-thick region of significantly reduced water density and hence fewer van der Waals attractions. These results are consistent with efforts examining the effects of LJ attractions (53) and introduction of charges (92) on the association of idealized nanoscale plates.

The difference in sign of $\Delta\Delta G_{rep}$ for the two interfaces is more complex, but can be understood as the excluded volume contribution that, for small solutes, is strongly tied to water's density fluctuations (21, 43, 81), with $\Delta\Delta G_{rep}$ approximately given by the cavity formation probability, $k_BT \ln P(N = 0)$. In the Gaussian approximation, enhancements to $P(N = 0)$ at surfaces result from either reduced water density or increased water density variance (21, 82). *SI Appendix*, Fig. S9 demonstrates that $-k_BT \ln P(N = 0)$ for a methane-sized volume [related to the hard-sphere methane chemical potential (43)] can decrease near the hydrophilic interface due to increased water density variance, while the same occurs at the hydrophobic interface due to decreased water density. At the hydroxyl surface, $\Delta\Delta G_{rep}$ values are still net positive, owing to averaging over the entire binding region, but it is notable that their contribution becomes small since some regions do show enhanced water density fluctuations. This is likely associated with decreased water entropy compared to bulk, as hydrogen bonding with a flat interface constrains water configurations similar to protein binding cavities (48, 49), although in a much less restrictive manner.

For comparison to current methods in membrane engineering, we examine the relation of free energy decompositions to Hansen solubility parameters (HSPs), which are experimentally determined molecular descriptors widely used to predict partitioning, solvation, and other solute solution properties for many applications, including membranes. HSPs deconstruct solvation energetic contributions into dispersion, polar, and hydrogen-bonding contributions (95, 96). Here, we develop a penalized regression model (*SI Appendix*) based on HSPs that fits MD binding free energies well ($R^2 = 0.886$), and that selects relevant descriptors as 1) the dispersion HSP, δ_d; 2) the polar HSP, δ_p; 3) an intercept term representing the mean ΔG_{bind} for the –OH surface; and 4) a conditional offset that represents the average ΔG_{bind} shift when changing to a $-CH_3$ surface. Like Fig. 3 *A* and *B*, this regression reveals a competition between LJ contributions probed by δ_d, which favor binding, and electrostatics probed by δ_p, which disfavor it. While the model cannot capture the flipped signs of binding contributions differentiating hydroxylated and methylated surfaces, and all surface differences are lumped into the conditional offset, this averaging approach approximately captures overall surface-dependent binding trends. Still, we expect a single surface-dependent offset to have limited use in capturing binding properties of larger solutes, as regression errors appear to grow with solute size. Moreover, as we show in the next section, patterned surfaces lead to more complicated surface dependencies and even allow for manipulation of solute selectivity not predicted by such linear regression models.

A complementary and insightful perspective on surface-binding driving forces instead decomposes the free energy of solvation as $\Delta G_{solv} = \langle U_{sw}\rangle_2 + S_{rel,1\to2}$. As shown in ref. 97, $\langle U_{sw}\rangle_2$ reports the average interactions (potential energies) of the solute with other species in the system (i.e., water and interface) and hence the direct energetic contributions to solvation. $S_{rel,1\to2}$ then is the relative entropy associated with solvating the solute; it is always positive and assesses how a system's conformational fluctuations adapt to perturbations (97). This approach is similar in spirit to inhomogeneous solvation theory (98) and associated methods that predict free energies of binding based on shifts in water structure (48, 49). However, the contributing terms are fundamentally distinct (97), avoiding cancelation between energetic and entropic terms (99, 100). Importantly, for relatively rigid solutes and surfaces, this relative entropy measures the penalty due to a solute's perturbation of water's fluctuating structure, and hence Eq. **3** more cleanly separates direct energetic and water structural contributions to solvation:

$$\Delta G_{bind} = \Delta\langle U_{sw}\rangle_2 + \Delta S_{rel,1\to2}. \quad [3]$$

A similar decomposition was earlier proposed (100), although it has not been recognized and interpreted as a relative entropy, which has fundamental connections to fluctuation theory, ensemble overlap, and nonequilibrium thermodynamics (101).

Fig. 3 *C* and *D* assesses the decomposition into direct energy $\Delta\langle U_{sw}\rangle_2$ and water restructuring $\Delta S_{rel,1\to2}$ contributions. For the methyl-terminated surfaces, the restructuring term contributes favorably and the mean solute–system energies resist binding.

This trend is reversed for the hydroxyl-terminated surfaces. This reveals the relative importance of direct energetics versus water structure at the two distinct interfaces for chemically diverse systems, in contrast to previous studies of simpler solutes and interfaces (41, 53, 87). There is a clear correspondence with the earlier discussed free energy decomposition; *SI Appendix*, Fig. S7 demonstrates that $\Delta S_{rel,1\to2}$ correlates with $\Delta\Delta G_{rep}$, while $\Delta\langle U_{sw}\rangle_2$ tracks the sum of $\Delta\Delta G_{attr}$ and $\Delta\Delta G_Q$. However, the relative entropy more clearly delineates the unique response and role of water in the net solute–surface interactions. Along these lines, we can decompose PMFs into distance-dependent $\Delta\langle U_{sw}\rangle_2$ and $\Delta S_{rel,1\to2}$ contributions. *SI Appendix*, Figs. S10 and S11 reveal that indeed the relative entropy drives affinity at the hydrophobic interface while more favorable solute–system potential energies drive affinity near the hydrophilic one. This result reinforces the crossover in driving forces seen in Fig. 3 when moving from the methylated to the hydroxylated interface.

Discovery of High-Affinity, Chemically Patterned Surfaces with Genetic Algorithm Optimization. Beyond the homogeneous surfaces considered thus far, heterogeneous interfaces involving multiple chemical groups (e.g., mixed –OH, –CH_3 SAMs) impact solute affinity in less understood ways, where the spatial organization of groups represents an additional surface feature that can be engineered to impact membrane selectivity and fouling resistance. Previous work has demonstrated that patterning of flat interfaces impacts affinity of idealized solutes (21), as well as the related dewetting behavior of interfacial water (22, 23, 92). The combination of heterogeneous geometry and chemistry exhibited by proteins produces an even more complex water response (52, 55, 62, 63) and nonobvious trends in the binding of idealized hydrophobic solutes (46, 47).

Here, we focus on the role of functional group patterning at geometrically simple interfaces, allowing us to specifically identify how chemical heterogeneities impact realistic solutes of varying chemistries. We use a genetic optimization algorithm to guide exploration of the headgroup pattern design space by identifying where simulations should be performed and discovering surfaces with either minimal or maximal solute–surface binding affinities. To optimize affinity, it is only necessary to optimize ΔG^{surf}_{solv} because the bulk solvation term in Eq. **1** is constant across surface modifications. We previously used a computational evolution strategy to repattern surfaces to manipulate water mobility (25). In the present work, we enhance this approach using on-the-fly machine-learned estimates of ΔG_{bind} that greatly reduce computational cost, which is necessary to make optimization viable for the computationally expensive binding free energy calculations. We find that in simple cases (e.g., mixed methyl–hydroxyl surfaces), the optima generated by the genetic algorithm are not unlike idealized patterns that might be anticipated by rational exploration. In more complex cases, such as those involving three surface chemistries discussed later, the resulting optimal motifs are less obvious in advance, but still suggest idealized patterns that should be characterized. It is clear that for more complex surfaces (e.g., fouling-resistant membranes for water treatment involving many types of functional groups) and optimization targets (e.g., selectivities involving multiple types of solutes), optimal patterns will not be easily intuitable and the genetic algorithm will be critical.

As a base case, we first optimize the affinity of methane to a SAM interface of equal numbers of methyl and hydroxyl headgroups. *SI Appendix*, Fig. S12 shows the progress of the genetic algorithm, while Fig. 4*A* gives resulting patterns: a surface with a single large patch of hydrophobic groups minimizes the surface solvation free energy (increases density fluctuations) and maximizes methane affinity, while a surface with dispersed hydrophobic groups

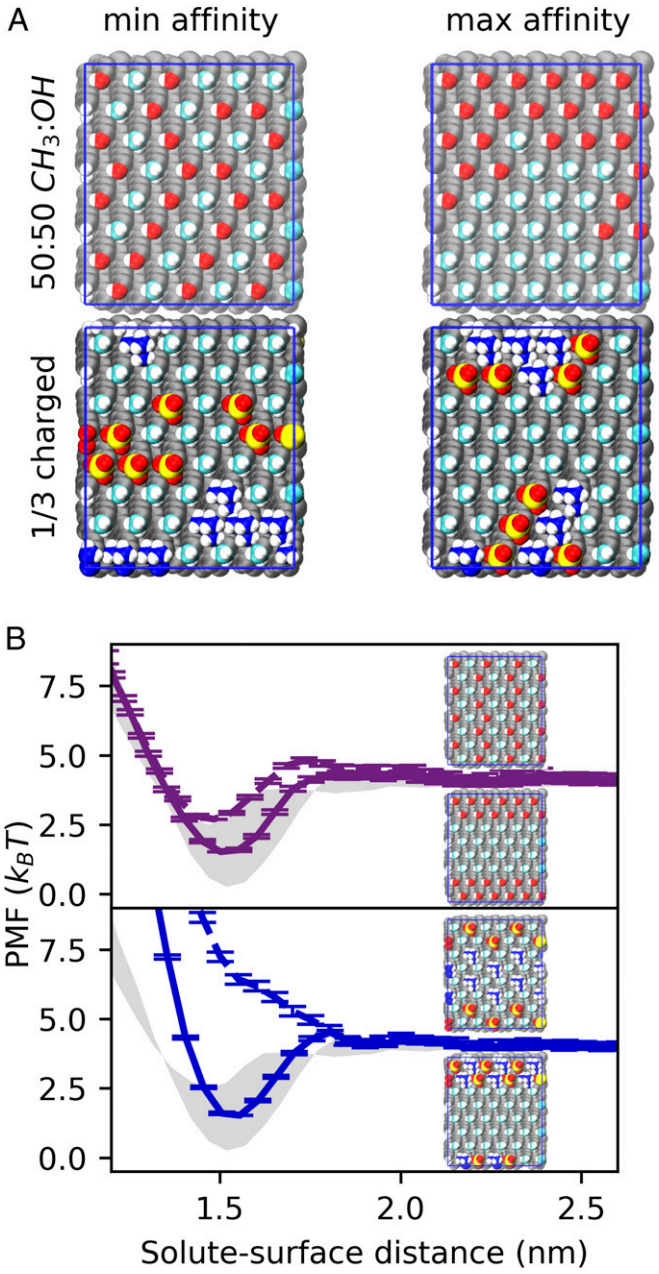

Fig. 4. (*A*) Minimum and maximum binding free energy surface representations from genetic algorithm optimizations of methane affinity. The *Top* images involve repatterning of hydroxyl and methyl groups, while the *Bottom* involve charged headgroups (quaternary ammonium and sulfonate) patterns on a methyl background. (*B*) Methane PMFs and *Inset* surface images for idealized spread (dashed) and patchy (solid) patterns of CH_3/OH headgroups. The *Bottom* panel shows methane PMFs for spread–patch (dashed) and patch–spread (solid) patterns of charged headgroups. The shaded gray regions represent areas between fully hydroxylated and methylated PMFs for methane shown in Fig. 2.

maximizes solvation free energy (decreases density fluctuations) and minimizes affinity. The optimization results suggest that idealized patchy and dispersed surfaces, shown in Fig. 4*B*, are the true global optima. These results are consistent with earlier studies showing hydrophobic group clustering enhances density fluctuations (20, 21, 92) and accelerates water dynamics at an interface (25), but importantly involve direct optimization of affinity, without underlying assumptions about the relevant physical driving forces.

Assuming water density fluctuations are the primary factor determining small solute affinity for interfaces, we expect that similar patterns as found for methane will maximize and minimize the interfacial ΔG_{solv}^{surf} for the broader set of solutes. This hypothesis is consistent with differences between affinities of solutes to the perfect "patchy" and "spread" patterns (Fig. 4*B*, *Insets*) as shown in Table 2. To further test this idea, we apply the genetic algorithm to extremize the affinity of both benzene, a model aromatic hydrophobe, and capped glycine, a larger and more flexible solute, via surface patterning. In both cases, the genetic algorithm discovers similar surface patterns as for methane, concretely demonstrating that the same principles that improve affinity of small, idealized solutes (20, 21) can also be applied to more complex small molecules.

While the hydroxyl and methyl interfaces show favorable (negative) binding free energies, surfaces with charged sites are thought to tightly bind water that resists adsorption of neutral solutes (10). To understand such effects, we examine SAMs with quaternary ammonium (+1) and sulfonate (−1) headgroups, chemistries commonly used to increase interfacial fouling resistance (102). As an instructive case, we consider surfaces covered in a third of these groups, in equal numbers to maintain charge neutrality, while the remaining two-thirds of sites are methyl. We use the genetic algorithm to minimize and maximize affinity for ammonia, methane, methanol, benzene, and phenol at such interfaces, with the results summarized in *SI Appendix*, Tables S7–S11 and Figs. S15–S19. Maximum affinity for all solutes occurs when charged headgroups are well mixed in a single cluster (Fig. 4*A*). In the minimum affinity case, charged groups are dispersed on the surface, in segregated domains of opposite charge (Fig. 4*A*). The genetic algorithm is critical in this discovery because these optimized surfaces are less intuitive than the hydroxyl/methyl case as the increased number of headgroup chemistries expands the number and complexity of the set of possible patterns.

Informed by the optimization results, we study four idealized surfaces involving charged headgroups (shown in Fig. 4*B* and *SI Appendix*, Tables S7–S11): charged groups clustered but subsegregated by charge (patch–patch), charged groups clustered and internally mixed (patch–spread), charged groups dispersed but within regions of like charge (spread–patch), and charged groups dispersed with opposite charges interspersed (spread–spread). *SI Appendix*, Figs. S8 and S9 indeed show that waters more tightly adhere to a charged interface, with higher density and lower density fluctuations; the effect is strongest for the spread–patch configuration. On such interfaces, PMFs become completely repulsive, while creation of large patches of methyl groups reintroduces favorable affinity (Fig. 4*B*). Similar induction of repulsive interactions via surface charge has been observed between extended plates (92) and binding of simple hydrophobes to model cavities (83). For all solutes except ammonia, the patch–spread configuration gives maximum affinity and the spread–patch arrangement minimum. For ammonia, the spread–spread surface has a slightly lower affinity than the spread–patch configuration, due to favorable electrostatics (*SI Appendix*, Fig. S6).

Surface Patterns Modulate Water Density Fluctuations to Adjust Affinity and Selectivity. To what extent can surface patterning influence solute–surface affinity? Table 2 compares differences between solvation free energies at the perfectly dispersed and patchy interfaces with 1:1 methyl/hydroxyl headgroups to differences between the "pure," fully hydroxylated and methylated interfaces. Consistent with water density fluctuations near pure interfaces, patchy surfaces produce higher relative water density fluctuations and always lower solvation free energies (higher affinities) than the corresponding binding scenarios for spread surfaces of the same composition, even for the previously unexplored case of polar solutes. Moreover, the effect of patterning is significant for all solutes; it achieves a variation in binding affinity merely due to spatial group arrangement that is 19 to 50% of the range between the purely methylated to hydroxylated interfaces. While pattern-induced variations are all less than 2 k_BT, this corresponds to nearly a sevenfold change in surface concentration. Since the affinity differences in Table 2 scale with solute size, one might expect that patterning becomes more significant for larger solutes, although the role of density fluctuations in such cases may also diminish (86).

On the other hand, the interfaces with charged headgroups show much larger patterning effects. In fact, the binding free energy of benzene changes sign from −3.33 k_BT on the patch–spread

Table 2. Differences in binding free energies at various interfaces, in units of k_BT

Solute	$\Delta G_{bind}^{OH} - \Delta G_{bind}^{CH_3}$	50:50 CH_3:OH, spread – patch	f 50:50 CH_3:OH, spread – patch	1/3 charged, spread-patch –patch-spread	f 1/3 charged, spread-patch –patch-spread
Ammonia	0.73 ± 0.07 (5.50×10^{-5})	0.37 ± 0.06 (1.74×10^{-4})	0.50 ± 0.09	0.52 ± 0.08 (3.70×10^{-4})	0.72 ± 0.13
Benzene	3.22 ± 0.10 (1.35×10^{-9})	1.62 ± 0.15 (9.26×10^{-6})	0.50 ± 0.05	5.76 ± 0.10 (3.40×10^{-9})	1.79 ± 0.07
Boric acid	0.87 ± 0.13 (8.02×10^{-4})	0.42 ± 0.14 (1.50×10^{-2})	0.48 ± 0.17	—	—
Capped glycine	2.46 ± 0.21 (3.03×10^{-6})	0.94 ± 0.25 (6.13×10^{-3})	0.38 ± 0.11	—	—
Isopropanol	2.66 ± 0.08 (1.13×10^{-9})	1.07 ± 0.15 (1.93×10^{-4})	0.40 ± 0.06	—	—
Methane	2.32 ± 0.06 (6.43×10^{-8})	0.96 ± 0.04 (5.93×10^{-8})	0.41 ± 0.02	3.99 ± 0.08 (7.19×10^{-9})	1.72 ± 0.05
Methanol	1.60 ± 0.13 (2.03×10^{-4})	0.50 ± 0.09 (6.10×10^{-4})	0.31 ± 0.06	1.84 ± 0.10 (5.10×10^{-6})	1.15 ± 0.11
Phenol	3.39 ± 0.13 (7.62×10^{-8})	1.50 ± 0.10 (5.90×10^{-7})	0.44 ± 0.04	4.70 ± 0.17 (1.20×10^{-8})	1.38 ± 0.07

$f = (\Delta G_{bind}^{i} - \Delta G_{bind}^{j})/(\Delta G_{bind}^{OH} - \Delta G_{bind}^{CH_3})$ represents the ratio of the binding free energy difference between two patterned surfaces to the difference between the purely hydroxylated and methylated interfaces shown in the first column. Errors are based on SE propagation of the SE in the mean from five independent MD simulation runs. Numbers in parentheses provide the *P* value for the two-sided hypothesis test for the equivalence of the mean binding free energies. Binding at the interfaces with charged groups was not performed for boric acid, capped glycine, or isopropanol.

surface to 2.43 k_BT (unfavorable) on the spread–patch surface—corresponding to a ∼300-fold reduction in surface concentration. This indicates that the arrangement of charged headgroups magnifies the impact of surface patterning on binding affinity, allowing surfaces with even a majority of hydrophobic headgroups to manifest a completely repulsive PMF (Fig. 4*B*). As with the hydroxylated patterns, differences with patterning are not as significant for small, polar solutes such as ammonia and methanol, but are still larger than for the methyl/hydroxyl interfaces.

What drives the effects of patterning and the manner by which charged groups magnify its role? *SI Appendix*, Figs. S5 and S6 demonstrate that all surfaces with large hydrophobic patches, regardless of the presence of hydroxyl or charged headgroups, drive solute–surface affinity through the repulsive contribution to the solvation free energy, even for polar solutes, similar to what we observed for the methyl and hydroxyl surfaces as well as for prior studies with more model solutes and interfaces (41, 53, 87). With fully charged solutes, however, this trend may eventually invert with direct attractions to charged surface sites. On the other hand, surfaces with distributed methyls show distinct driving forces depending on the complementary polar groups (hydroxyl or charged). For the spread methyl–hydroxyl surfaces, the water restructuring penalty $\Delta S_{rel,1\to2}$ drives favorable binding for all solutes. In contrast for the methyl-charged surfaces, the spread–patch and spread–spread arrangements make solute binding unfavorable in every case. $\Delta S_{rel,1\to2}$ is again responsible, but in this case with positive values (*SI Appendix*, Fig. S6) that are greater than for the purely hydroxylated interface (Fig. 3).

Interestingly, surfaces with dispersed charges are the only interfaces with a favorable electrostatic contribution to affinity (*SI Appendix*, Fig. S6), which holds for all solutes but grows larger for the more polar ones. These surface patterns also increase water density (*SI Appendix*, Fig. S8) and simultaneously greatly reduce density fluctuations (*SI Appendix*, Fig. S9), as also seen in more idealized charged systems (92), which together demonstrate tighter surface adherence of water. Such strong adherence results in high water reorganizational penalties and accordingly unfavorable $\Delta S_{rel,1\to2}$, resulting in completely repulsive PMFs (Fig. 4*B*). Clustering charged groups and exposing large hydrophobic regions removes this effect, resulting in $\Delta S_{rel,1\to2}$ driving binding and the reappearance of PMF minima.

Shifts in chemical patterning appear to affect polar solutes less than nonpolar ones. Such differences are present to varying degrees among all solutes, even between nonpolar entities, reinforcing the idea that hydrophobic characterization of interfaces based on chemical potentials of repulsive probes varies with the size and shape of the probe (46, 93). This differential response of distinct solutes suggests the possibility to design surface patterns to select between solutes. We define selectivity by the ratio of the surface concentration of solute 2 to that of solute 1 for the same dilute bulk concentration, which follows:

$$\frac{C_2/C_{bulk}}{C_1/C_{bulk}} = \frac{e^{-(\beta\Delta G_{bind,2})}}{e^{-(\beta\Delta G_{bind,1})}} = \frac{e^{-(\beta\Delta G_{solv,2}-\Delta G_{bulk,2})}}{e^{-(\beta\Delta G_{solv,1}-\Delta G_{bulk,1})}}, \quad [4]$$

where the second equality uses Eq. **1**. Bulk solvation free energies are unaffected by the patterning, so selectivity is optimized by targeting the difference in the surface solvation free energies. Because this difference increases more dramatically with surface patchiness for larger and more hydrophobic solutes, we expect patchy patterns to make such interfaces more selective for such solutes. *SI Appendix*, Table S12 shows surfaces from genetic algorithm optimization of selectivity for methanol compared to methane. Indeed, methanol selectivity is minimized for a patchy arrangement and maximized for dispersed hydroxyls, with computed binding free energy differences (methanol minus methane) of 0.42 and 0.21 k_BT (*SI Appendix*, Table S12).

Conclusions

We use simulation free energy calculations to investigate fundamental determinants of surface binding affinity by examining a broad space of chemically diverse small solutes and surfaces. First, we find that nearly all solutes considered—apolar and polar—display affinity to both methyl and hydroxyl surfaces. Second, we find that surface affinity is poorly correlated to conventional measures of solute hydrophobicity, as evaluated by either hydration free energies or octanol–water transfer partition coefficients. Instead, decompositions of the binding free energy suggest the origins of surface affinity in terms of specific interactions and water restructuring, highlighting the role of surface water density fluctuations. At methyl interfaces, solute affinity is driven by a relative entropy contribution that captures penalties from solute-induced water structural rearrangements, while direct attractive solute–surface interactions dominate affinity at hydroxylated interfaces. These results demonstrate the relevance of molecular descriptors of hydrophobicity across a broad chemical spectrum.

Moving to heterogeneous surfaces, we show that interfacial affinity is also modulated by surface functional group spatial patterning and develop an optimization algorithm to tune affinity (or selectivity) by patterning surfaces. We find that surfaces with segregated domains of hydrophobic and hydrophilic (polar or charged) headgroups maximize solute affinity, while those with well-mixed patterns minimize it. Moreover, varying charged headgroup arrangements on a hydrophobic background can switch surfaces from strongly repulsive to attractive, inverting the sign of the binding free energy. Notably, shifts in binding affinity due to patterning are proportional to the solute volume and overall surface affinity, meaning that such patterns may also modify the selectivity of an interface to one solute versus another. Here, we do not evaluate the role of surface flexibility or curvature in determining solute surface affinity, instead developing a necessary baseline to understand the effect of chemical heterogeneity on a set of chemically diverse solutes. Such knowledge becomes a crucial control when considering geometric roughness and fluctuations relevant to both membranes and biomolecules, as expected from earlier efforts that show how flexibility and convexity impact affinity (11, 12, 60, 61, 83, 103).

The present results suggest design strategies and opportunities in interfacial materials for water purification membranes, but also in chromatography, catalysis, and many other applications involving water-mediated solute–surface interactions. Design trade-offs are likely; for example, surface patterns that minimize solute affinity are likely to also minimize water dynamics (25), which in membrane applications suggests an affinity-transport trade-off. An obvious extension of this approach is to charged solutes, as well as interfaces with net charge and counterions in solution that may compete for binding, in which case density fluctuations may not dominate surface affinity.

Data Availability. All data are included in the article and SI Appendix. Code used to generate and analyze data is publicly available on GitHub at https://github.com/JIMonroe/Surface_Affinities_Optimization.

ACKNOWLEDGMENTS. This work was supported as part of the Center for Materials for Water and Energy Systems, an Energy Frontier Research Center funded by the US Department of Energy, Office of Science, Basic Energy Sciences under Award DE-SC0019272. We are thankful for computational resources provided by the Center for Scientific Computing supported by the California NanoSystems Institute and the Materials Research Science and Engineering Center at University of California, Santa Barbara, through NSF Division of Materials Research Award 1720256 and NSF Division of Computer and Network Systems Award 1725797. J.I.M. acknowledges support from the NSF Graduate Research Fellowship (Division of Graduate Education [DGE] Award 1144085). S.J. acknowledges support from the NSF Graduate Research Fellowship (DGE Award 1650114).

1. K. Arai, R. Bhatia, S. Kapoor, Eds. *Proceedings of the Future Technologies Conference (FTC)*, Vol. 1 (Springer Nature, 2019).
2. J. R. Werber, C. O. Osuji, M. Elimelech, Materials for next-generation desalination and water purification membranes. *Nat. Rev. Mater.* **1**, 16018 (2016).
3. H. B. Park, J. Kamcev, L. M. Robeson, M. Elimelech, B. D. Freeman, Maximizing the right stuff: The trade-off between membrane permeability and selectivity. *Science* **356**, eaab0530 (2017).
4. C. Fritzmann, J. Löwenberg, T. Wintgens, T. Melin, State-of-the-art of reverse osmosis desalination. *Desalination* **216**, 1–76 (2007).
5. D. J. Miller, D. R. Dreyer, C. W. Bielawski, D. R. Paul, B. D. Freeman, Surface modification of water purification membranes. *Angew. Chem. Int. Ed. Engl.* **56**, 4662–4711 (2017).
6. E. Ostuni, R. G. Chapman, R. E. Holmlin, S. Takayama, G. M. Whitesides, A survey of structure–property relationships of surfaces that resist the adsorption of protein. *Langmuir* **17**, 5605–5620 (2001).
7. J. L. Dalsin, P. B. Messersmith, Bioinspired antifouling polymers. *Mater. Today* **8**, 38–46 (2005).
8. D. Rana, T. Matsuura, Surface modifications for antifouling membranes. *Chem. Rev.* **110**, 2448–2471 (2010).
9. G. D. Kang, Y. M. Cao, Development of antifouling reverse osmosis membranes for water treatment: A review. *Water Res.* **46**, 584–600 (2012).
10. M. Elimelech, W. A. Phillip, The future of seawater desalination: Energy, technology, and the environment. *Science* **333**, 712–717 (2011).
11. L. Li, S. Chen, J. Zheng, B. D. Ratner, S. Jiang, Protein adsorption on oligo(ethylene glycol)-terminated alkanethiolate self-assembled monolayers: The molecular basis for nonfouling behavior. *J. Phys. Chem. B* **109**, 2934–2941 (2005).
12. A. E. Ismail, G. S. Grest, M. J. Stevens, Structure and dynamics of water near the interface with oligo(ethylene oxide) self-assembled monolayers. *Langmuir* **23**, 8508–8514 (2007).
13. J. Imbrogno, M. D. Williams, G. Belfort, A new combinatorial method for synthesizing, screening, and discovering antifouling surface chemistries. *ACS Appl. Mater. Interfaces* **7**, 2385–2392 (2015).
14. T. C. Le, M. Penna, D. A. Winkler, I. Yarovsky, Quantitative design rules for protein-resistant surface coatings using machine learning. *Sci. Rep.* **9**, 265 (2019).
15. S. Krishnan, C. J. Weinman, C. K. Ober, Advances in polymers for anti-biofouling surfaces. *J. Mater. Chem.* **18**, 3405 (2008).
16. E. Ostuni, B. A. Grzybowski, M. Mrksich, C. S. Roberts, G. M. Whitesides, Adsorption of proteins to hydrophobic sites on mixed self-assembled monolayers. *Langmuir* **19**, 1861–1872 (2003).
17. M. Penna, K. Ley, S. Maclaughlin, I. Yarovsky, Surface heterogeneity: A friend or foe of protein adsorption—insights from theoretical simulations. *Faraday Discuss.* **191**, 435–464 (2016).
18. J. Comer, R. Chen, H. Poblete, A. Vergara-Jaque, J. E. Riviere, Predicting adsorption affinities of small molecules on carbon nanotubes using molecular dynamics simulation. *ACS Nano* **9**, 11761–11774 (2015).
19. W. van Zoelen *et al*., Sequence of hydrophobic and hydrophilic residues in amphiphilic polymer coatings affects surface structure and marine antifouling/fouling release properties. *ACS Macro Lett.* **3**, 364–368 (2014).
20. S. N. Jamadagni, R. Godawat, S. Garde, Hydrophobicity of proteins and interfaces: Insights from density fluctuations. *Annu. Rev. Chem. Biomol. Eng.* **2**, 147–171 (2011).
21. H. Acharya, S. Vembanur, S. N. Jamadagni, S. Garde, Mapping hydrophobicity at the nanoscale: Applications to heterogeneous surfaces and proteins. *Faraday Discuss.* **146**, 353–365, discussion 367–393, 395–401 (2010).
22. N. Giovambattista, P. G. Debenedetti, P. J. Rossky, Hydration behavior under confinement by nanoscale surfaces with patterned hydrophobicity and hydrophilicity. *J. Phys. Chem. C* **111**, 1323–1332 (2007).
23. N. Giovambattista, P. J. Rossky, P. G. Debenedetti, Effect of temperature on the structure and phase behavior of water confined by hydrophobic, hydrophilic, and heterogeneous surfaces. *J. Phys. Chem. B* **113**, 13723–13734 (2009).
24. N. Giovambattista, P. J. Rossky, P. G. Debenedetti, Computational studies of pressure, temperature, and surface effects on the structure and thermodynamics of confined water. *Annu. Rev. Phys. Chem.* **63**, 179–200 (2012).
25. J. I. Monroe, M. S. Shell, Computational discovery of chemically patterned surfaces that effect unique hydration water dynamics. *Proc. Natl. Acad. Sci. U.S.A.* **115**, 8093–8098 (2018).
26. T. Abramyan *et al*., Understanding protein-surface interactions at the atomistic level through the synergistic development of experimental and molecular simulation methods. *ACS Symp. Ser.* **1120**, 197–228 (2012).
27. N. A. Vellore, J. A. Yancey, G. Collier, R. A. Latour, S. J. Stuart, Assessment of the transferability of a protein force field for the simulation of peptide-surface interactions. *Langmuir* **26**, 7396–7404 (2010).
28. Z. A. Levine *et al*., Surface force measurements and simulations of Mussel-derived peptide adhesives on wet organic surfaces. *Proc. Natl. Acad. Sci. U.S.A.*, 201603065 (2016).
29. P. Stock *et al*., Unraveling hydrophobic interactions at the molecular scale using force spectroscopy and molecular dynamics simulations. *ACS Nano* **11**, 2586–2597 (2017).
30. M. Deighan, J. Pfaendtner, Exhaustively sampling peptide adsorption with metadynamics. *Langmuir* **29**, 7999–8009 (2013).
31. Y. Xie, M. Liu, J. Zhou, Molecular dynamics simulations of peptide adsorption on self-assembled monolayers. *Appl. Surf. Sci.* **258**, 8153–8159 (2012).
32. S. N. Jamadagni, R. Godawat, S. Garde, How surface wettability affects the binding, folding, and dynamics of hydrophobic polymers at interfaces. *Langmuir* **25**, 13092–13099 (2009).
33. A. Prakash, K. G. Sprenger, J. Pfaendtner, Essential slow degrees of freedom in protein-surface simulations: A metadynamics investigation. *Biochem. Biophys. Res. Commun.* **498**, 274–281 (2018).
34. J.-W. Shen, T. Wu, Q. Wang, H.-H. Pan, Molecular simulation of protein adsorption and desorption on hydroxyapatite surfaces. *Biomaterials* **29**, 513–532 (2008).
35. M. Mijajlovic, M. J. Penna, M. J. Biggs, Free energy of adsorption for a peptide at a liquid/solid interface via nonequilibrium molecular dynamics. *Langmuir* **29**, 2919–2926 (2013).
36. G. H. Zerze, R. G. Mullen, Z. A. Levine, J. E. Shea, J. Mittal, To what extent does surface hydrophobicity dictate peptide folding and stability near surfaces? *Langmuir* **31**, 12223–12230 (2015).
37. Z. W. Ulissi, J. Zhang, V. Sresht, D. Blankschtein, M. S. Strano, 2D equation-of-state model for corona phase molecular recognition on single-walled carbon nanotube and graphene surfaces. *Langmuir* **31**, 628–636 (2015).
38. E. R. Azhagiya Singam *et al*., Thermodynamics of adsorption on graphenic surfaces from aqueous solution. *J. Chem. Theory Comput.* **15**, 1302–1316 (2019).
39. X.-R. Xia, N. A. Monteiro-Riviere, J. E. Riviere, An index for characterization of nanomaterials in biological systems. *Nat. Nanotechnol.* **5**, 671–675 (2010).
40. O. G. Apul, T. Karanfil, Adsorption of synthetic organic contaminants by carbon nanotubes: A critical review. *Water Res.* **68**, 34–55 (2015).
41. A. Wallqvist, B. J. Berne, Hydrophobic interaction between a methane molecule and a paraffin wall in liquid water. *Chem. Phys. Lett.* **145**, 26–32 (1988).
42. A. J. Patel *et al*., Extended surfaces modulate hydrophobic interactions of neighboring solutes. *Proc. Natl. Acad. Sci. U.S.A.* **108**, 17678–17683 (2011).
43. R. Godawat, S. N. Jamadagni, S. Garde, Characterizing hydrophobicity of interfaces by using cavity formation, solute binding, and water correlations. *Proc. Natl. Acad. Sci. U.S.A.* **106**, 15119–15124 (2009).
44. L. Hua, X. Huang, P. Liu, R. Zhou, B. J. Berne, Nanoscale dewetting transition in protein complex folding. *J. Phys. Chem. B* **111**, 9069–9077 (2007).
45. A. J. Patel *et al*., Sitting at the edge: How biomolecules use hydrophobicity to tune their interactions and function. *J. Phys. Chem. B* **116**, 2498–2503 (2012).
46. A. J. Patel, S. Garde, Efficient method to characterize the context-dependent hydrophobicity of proteins. *J. Phys. Chem. B* **118**, 1564–1573 (2014).
47. R. Barnes *et al*., Spatially heterogeneous surface water diffusivity around structured protein surfaces at equilibrium. *J. Am. Chem. Soc.* **139**, 17890–17901 (2017).
48. T. Young, R. Abel, B. Kim, B. J. Berne, R. A. Friesner, Motifs for molecular recognition exploiting hydrophobic enclosure in protein-ligand binding. *Proc. Natl. Acad. Sci. U.S.A.* **104**, 808–813 (2007).
49. R. Abel, L. Wang, R. A. Friesner, B. J. Berne, A displaced-solvent functional analysis of model hydrophobic enclosures. *J. Chem. Theory Comput.* **6**, 2924–2934 (2010).
50. A. P. Willard, D. Chandler, Instantaneous liquid interfaces. *J. Phys. Chem. B* **114**, 1954–1958 (2010).
51. C. G. Ricci, J. A. McCammon, Heterogeneous solvation in distinctive protein-protein interfaces revealed by molecular dynamics simulations. *J. Phys. Chem. B* **122**, 11695–11701 (2018).
52. N. Giovambattista, C. F. Lopez, P. J. Rossky, P. G. Debenedetti, Hydrophobicity of protein surfaces: Separating geometry from chemistry. *Proc. Natl. Acad. Sci. U.S.A.* **105**, 2274–2279 (2008).
53. N. Choudhury, B. M. Pettitt, On the mechanism of hydrophobic association of nanoscopic solutes. *J. Am. Chem. Soc.* **127**, 3556–3567 (2005).
54. N. Choudhury, B. M. Pettitt, Enthalpy-entropy contributions to the potential of mean force of nanoscopic hydrophobic solutes. *J. Phys. Chem. B* **110**, 8459–8463 (2006).
55. R. Zhou, X. Huang, C. J. Margulis, B. J. Berne, Hydrophobic collapse in multidomain protein folding. *Science* **305**, 1605–1609 (2004).
56. R. C. Harris, J. A. Drake, B. M. Pettitt, Multibody correlations in the hydrophobic solvation of glycine peptides. *J. Chem. Phys.* **141**, 22D525 (2014).
57. R. C. Harris, B. M. Pettitt, Effects of geometry and chemistry on hydrophobic solvation. *Proc. Natl. Acad. Sci. U.S.A.* **111**, 14681–14686 (2014).
58. R. C. Harris, B. M. Pettitt, Reconciling the understanding of "hydrophobicity" with physics-based models of proteins. *J. Phys. Condens. Matter* **28**, 083003 (2016).
59. H. Acharya, N. J. Mozdzierz, P. Keblinski, S. Garde, How chemistry, nanoscale roughness, and the direction of heat flow affect thermal conductance of solid-water interfaces. *Ind. Eng. Chem. Res.* **51**, 1767–1773 (2012).
60. E. Xi *et al*., Hydrophobicity of proteins and nanostructured solutes is governed by topographical and chemical context. *Proc. Natl. Acad. Sci. U.S.A.* **114**, 13345–13350 (2017).
61. P. Setny, Water properties and potential of mean force for hydrophobic interactions of methane and nanoscopic pockets studied by computer simulations. *J. Chem. Phys.* **127**, 054505 (2007).
62. Y.-K. Cheng, P. J. Rossky, Surface topography dependence of biomolecular hydrophobic hydration. *Nature* **392**, 696–699 (1998).
63. N. Giovambattista, P. G. Debenedetti, P. J. Rossky, Enhanced surface hydrophobicity by coupling of surface polarity and topography. *Proc. Natl. Acad. Sci. U.S.A.* **106**, 15181–15185 (2009).
64. P. Jungwirth, D. J. Tobias, Specific ion effects at the air/water interface. *Chem. Rev.* **106**, 1259–1281 (2006).
65. N. Shenogina, R. Godawat, P. Keblinski, S. Garde, How wetting and adhesion affect thermal conductance of a range of hydrophobic to hydrophilic aqueous interfaces. *Phys. Rev. Lett.* **102**, 156101 (2009).
66. H. W. Horn *et al*., Development of an improved four-site water model for biomolecular simulations: TIP4P-Ew. *J. Chem. Phys.* **120**, 9665–9678 (2004).
67. D. A. Case *et al*., AMBER 2018 (University of California, San Francisco, 2018).

68. A. Jakalian, D. B. Jack, C. I. Bayly, Fast, efficient generation of high-quality atomic charges. AM1-BCC model: II. Parameterization and validation. *J. Comput. Chem.* **23**, 1623–1641 (2002).
69. J. A. Maier *et al*., ff14SB: Improving the accuracy of protein side chain and backbone parameters from ff99SB. *J. Chem. Theory Comput.* **11**, 3696–3713 (2015).
70. D. S. Otkidach, I. V. Pletnev, Conformational analysis of boron-containing compounds using Gillespie–Kepert version of molecular mechanics. *J. Mol. Struct. THEOCHEM* **536**, 65–72 (2001).
71. S. L. Mayo, B. D. Olafson, W. A. Goddard, DREIDING: A generic force field for molecular simulations. *J. Phys. Chem.* **94**, 8897–8909 (1990).
72. B. Chen, J. J. Potoff, J. I. Siepmann, Monte Carlo calculations for alcohols and their mixtures with alkanes. Transferable potentials for phase equilibria. 5. United-atom description of primary, secondary, and tertiary alcohols. *J. Phys. Chem. B* **105**, 3093–3104 (2001).
73. P. Eastman *et al*., OpenMM 7: Rapid development of high performance algorithms for molecular dynamics. *PLoS Comput. Biol.* **13**, e1005659 (2017).
74. S. Miyamoto, P. A. Kollman, Settle: An analytical version of the SHAKE and RATTLE algorithm for rigid water models. *J. Comput. Chem.* **13**, 952–962 (1992).
75. C. Andersen, Rattle: A "velocity" version of the shake algorithm for molecular dynamics calculations. *J. Comput. Phys.* **52**, 24–34 (1983).
76. G. M. Torrie, J. P. Valleau, Nonphysical sampling distributions in Monte Carlo free-energy estimation: Umbrella sampling. *J. Comput. Phys.* **23**, 187–199 (1977).
77. P. Lyubartsev, a. Martsinovski, S. V. Shevkunov, P. N. Vorontsov-Velyaminov, New approach to Monte Carlo calculation of the free energy: Method of expanded ensembles. *J. Chem. Phys.* **96**, 1776 (1992).
78. F. A. Escobedo, F. J. Martínez-Veracoechea, Optimized expanded ensembles for simulations involving molecular insertions and deletions. I. Closed systems. *J. Chem. Phys.* **127**, 174103 (2007).
79. M. R. Shirts, J. D. Chodera, Statistically optimal analysis of samples from multiple equilibrium states. *J. Chem. Phys.* **129**, 124105 (2008).
80. J. D. Weeks, D. Chandler, H. C. Andersen, Role of repulsive forces in determining the equilibrium structure of simple liquids. *J. Chem. Phys.* **54**, 5237–5247 (1971).
81. G. Hummer, S. Garde, A. E. García, A. Pohorille, L. R. Pratt, An information theory model of hydrophobic interactions. *Proc. Natl. Acad. Sci. U.S.A.* **93**, 8951–8955 (1996).
82. S. Sarupria, S. Garde, Quantifying water density fluctuations and compressibility of hydration shells of hydrophobic solutes and proteins. *Phys. Rev. Lett.* **103**, 037803 (2009).
83. L. Wang, R. A. Friesner, B. J. Berne, Competition of electrostatic and hydrophobic interactions between small hydrophobes and model enclosures. *J. Phys. Chem. B* **114**, 7294–7301 (2010).
84. D. Ben-Amotz, Water-mediated hydrophobic interactions. *Annu. Rev. Phys. Chem.* **67**, 617–638 (2016).
85. A. Ben-Naim, Standard thermodynamics of transfer. Uses and misuses. *J. Phys. Chem.* **82**, 792–803 (1978).
86. D. Chandler, Interfaces and the driving force of hydrophobic assembly. *Nature* **437**, 640–647 (2005).
87. D. E. Smith, A. D. J. Haymet, Free energy, entropy, and internal energy of hydrophobic interactions: Computer simulations. *J. Chem. Phys.* **1993**, 6445 (1993).
88. X. Huang, C. J. Margulis, B. J. Berne, Do molecules as small as neopentane induce a hydrophobic response similar to that of large hydrophobic surfaces? *J. Phys. Chem. B* **107**, 11742–11748 (2003).
89. N. Choudhury, On the manifestation of hydrophobicity at the nanoscale. *J. Phys. Chem. B* **112**, 6296–6300 (2008).
90. J. G. Dorsey, K. A. Dill, The molecular mechanism of retention in reversed-phase liquid chromatography. *Chem. Rev.* **89**, 331–346 (1989).
91. M. Kanduč, A. Schlaich, E. Schneck, R. R. Netz, Water-mediated interactions between hydrophilic and hydrophobic surfaces. *Langmuir* **32**, 8767–8782 (2016).
92. L. Hua, R. Zangi, B. J. Berne, Hydrophobic interactions and dewetting between plates with hydrophobic and hydrophilic domains. *J. Phys. Chem. C* **113**, 5244–5253 (2009).
93. A. J. Patel, P. Varilly, D. Chandler, Fluctuations of water near extended hydrophobic and hydrophilic surfaces. *J. Phys. Chem. B* **114**, 1632–1637 (2010).
94. L. Wang, B. J. Berne, R. A. Friesner, Ligand binding to protein-binding pockets with wet and dry regions. *Proc. Natl. Acad. Sci. U.S.A.* **108**, 1326–1330 (2011).
95. A. del P. Sánchez-Camargo, M. Bueno, F. Parada-Alfonso, A. Cifuentes, E. Ibáñez, Hansen solubility parameters for selection of green extraction solvents. *Trends Analyt. Chem.* **118**, 227–237 (2019).
96. C. M. Hansen, *Hansen Solubility Parameters: A User's Handbook* (CRC Press, ed. 2, 2007).
97. J. I. Monroe, M. S. Shell, Decoding signatures of structure, bulk thermodynamics, and solvation in three-body angle distributions of rigid water models. *J. Chem. Phys.* **151**, 094501 (2019).
98. T. Lazaridis, Inhomogeneous fluid approach to solvation thermodynamics. 1. Theory. *J. Phys. Chem. B* **102**, 3531–3541 (1998).
99. H.-A. Yu, M. Karplus, A thermodynamic analysis of solvation. *J. Chem. Phys.* **89**, 2366 (1988).
100. D. Ben-Amotz, Interfacial solvation thermodynamics. *J. Phys. Condens. Matter* **28**, 414013 (2016).
101. M. S. Shell, Coarse-graining with the relative entropy. *Adv. Chem. Phys.* **161**, 395–441 (2016).
102. L. Mi, S. Jiang, Integrated antimicrobial and nonfouling zwitterionic polymers. *Angew. Chem. Int. Ed. Engl.* **53**, 1746–1754 (2014).
103. L. Wang, R. A. Friesner, B. J. Berne, Hydrophobic interactions in model enclosures from small to large length scales: Non-additivity in explicit and implicit solvent models. *Faraday Discuss.* **146**, 247–262, discussion 283–298, 395–401 (2010).
104. R. Sander, Compilation of Henry's law constants (version 4.0) for water as solvent. *Atmos. Chem. Phys.* **15**, 4399–4981 (2015).